QUEEN'S UNIVERSITY BELFAST

Easily Accessible Rare-Earth-Containing Phosphonium Room-Temperature Ionic Liquids: EXAFS, Luminescence and Magnetic Properties

Alvarez Vicente, J., Dandil, S., Banerjee, D., Gunaratne, H. Q. N., Gray, S., Felton, S., Srinivasan, G., Kaczmarek, A. M., Van Deun, R., & Nockemann, P. (2016). Easily Accessible Rare-Earth-Containing Phosphonium Room-Temperature Ionic Liquids: EXAFS, Luminescence and Magnetic Properties. *Journal of Physical Chemistry B*, *120*(23), 5301–5311. https://doi.org/10.1021/acs.jpcb.6b03870

Published in:
Journal of Physical Chemistry B

Document Version:
Peer reviewed version

Queen's University Belfast - Research Portal:
Link to publication record in Queen's University Belfast Research Portal

Publisher rights
This document is the Accepted Manuscript version of a Published Work that appeared in final form in The Journla of Physical Chemistry B, copyright © 2016 American Chemical Society after peer review and technical editing by the publisher. To access the final edited and published work see
http://pubs.acs.org/doi/abs/10.1021/acs.jpcb.6b03870

General rights
Copyright for the publications made accessible via the Queen's University Belfast Research Portal is retained by the author(s) and / or other copyright owners and it is a condition of accessing these publications that users recognise and abide by the legal requirements associated with these rights.

Take down policy
The Research Portal is Queen's institutional repository that provides access to Queen's research output. Every effort has been made to ensure that content in the Research Portal does not infringe any person's rights, or applicable UK laws. If you discover content in the Research Portal that you believe breaches copyright or violates any law, please contact openaccess@qub.ac.uk.

Open Access
This research has been made openly available by Queen's academics and its Open Research team. We would love to hear how access to this research benefits you. – Share your feedback with us: http://go.qub.ac.uk/oa-feedback

Download date:28. May. 2024

Easily Accessible Rare-Earth-Containing Phosphonium Room-Temperature Ionic Liquids: EXAFS, Luminescence and Magnetic Properties

Jorge Alvarez-Vicente,[a] Sahra Dandil,[a,e] Dipanjan Banerjee,[c] H.Q. Nimal Gunaratne,[a] Suzanne Gray,[d] Solveig Felton,[d] Geetha Srinivasan,[a] Anna M. Kaczmarek,[b] Rik Van Deun,[*b] and Peter Nockemann[*a]

a School of Chemistry and Chemical Engineering, The QUILL Research Centre, David Keir Building, Queen's University Belfast, Stranmillis Road Belfast BT9 5AG, UK.
b L^3 – Luminescent Lanthanide Lab, Department of Inorganic and Physical Chemistry, Ghent University, Krijgslaan 281-S3, B-9000 Ghent, Belgium.
c Dutch-Belgian Beamline (DUBBLE), ESRF - The European Synchrotron, CS 40220, 38043 Grenoble Cedex 9, France
d Centre for Nanostructured Media, School of Mathematics and Physics, Queen's University Belfast, Belfast, BT7 1NN, UK.
e Current address: Chemical and Process Engineering Department, Engineering Faculty, Gulumbe Campus, Bilecik Seyh Edebali University, 11210 Bilecik, Turkey.

Phosphonium Ionic Liquids, Liquid Lanthanides, Luminescence, Magnetic Properties, EXAFS

ABSTRACT A range of liquid rare-earth chlorometallate complexes with alkyl-phosphonium cations, $[P_{666\,14}]^+$, has been synthesised and characterised. EXAFS confirmed the predominant liquid-state speciation of the $[LnCl_6]^{3-}$ ion in the series with Ln = Nd, Eu, Dy. The crystal structure of the shorter-alkyl-chain cation analogue $[P_{4444}]^+$ has been determined and exhibits a very large unit cell. The luminescence properties, with visible light emissions of the liquid Tb, Eu, Pr and Sm and the NIR emissions for the Nd and Er compounds were determined. The effective magnetic moments were measured and fitted for the Nd, Tb, Ho, Dy, Gd and Er samples.

Ionic liquids (ILs) have received great attention within the last decade due to their special properties such as their negligible vapour pressure, ionic conductivity, thermal stability and the ability to dissolve a range of organic and inorganic compounds.[1] Ionic liquids have found a multitude of applications ranging from green solvents and metal extractions to gas cleaning.[2-4] Their use in inorganic and materials chemistry has also been reported.[5,6] Metal-containing ionic liquids combine the properties of ionic liquids with the intrinsic properties of the metal incorporated.[7] Well-known metal-containing ionic liquids are the chlorometallate-based systems, which have recently been reviewed by Estager *et al.*[8] These chloroaluminate ionic liquids (ILs) are well studied and their catalytic properties are extensively used.[9,10] Friedel-Crafts-reactions in the chloroaluminate ILs are a good example of the applicability of this type of compounds, since the Lewis acidity can be adjusted for applications.[11] These compounds often show complex anionic equilibria in the liquid phase. Some of their potential applications are in catalysis or as key components for biomass processing.

Transition metals such as Co, Zn and many others have also been used to obtain metal-containing ionic liquids.[12-14] Lin *et al.* have reviewed some of these metal-containing ILs with imidazolium used as cation.[15] Another example of metal-containing ionic liquids are deep-eutectic-solvents with metals incorporated as anions or cations, firstly introduced by Abbott *et al*.[16] Yoshida *et al*. reported in 2005 room-temperature (RT) ionic liquids containing iron(III) ions based on 1-ethyl-3-methylimidazolium cations. This ionic liquid exhibited high conductivity and fluidity and characteristic magnetic properties due to the metal incorporated. Backer *et al.* have reported on iron-containing magnetic ionic liquids, which are good examples of these materials adding additional intrinsic properties such as magnetism.[17]

We have been the first to incorporate highly charged metals, the lanthanides(III), into an ionic liquid forming low-melting metal-containing ionic liquids.[18] These metal-containing ionic liquids consist of 1-butyl-3-methylimidazolium (C_4MIm) cations and heptathiocyanato lanthanate (III) anions with the general formula $[C_6MIm]_{5-x}[Ln(SCN)_{8-x}(H_2O)_x]$ (x = 0-2, C_6MIm = 1-hexyl-3-methylimidazolium) (Ln = lanthanide). For the synthesis of these lanthanide-containing ionic liquids, a simple metathesis reaction was applied and the physical properties of these compounds were determined. Depending of the degree of drying under vacuum, these ionic liquids could contain from none up to two water molecules.

Lanthanide compounds with $[C_2MIm]^+$ cations and picrate anions (salt or an ester of picric acid, a 2,4,6-trinitrophenol) have been characterised in the solid state. Again, the presence of coordinating water facilitates the formation of single crystals. The photo-luminescent properties of these materials have been investigated and techniques such as IR, elemental analysis and conductivity measurements have been used.[19] Mallick *et al.* have investigated the thiocyanato lanthanate ionic liquids containing dysprosium, which was chosen for this study due to its luminescent and magnetic properties.[20] A water-free rare-earth-containing ionic liquid, $[C_4MIm][Eu(Tf_2N)_4]$ was reported by Tang *et al.* and the photo-physical properties were investigated.[21]

Ionic liquids have also been used as solvents for lanthanide spectroscopy, and one of the advantages of this is that due to the low vapour pressure of ILs, these solutions can be dried at

high temperatures and under high vacuum, facilitating the removal of water coordinated to the lanthanide ions.[22,23] The elimination of coordinated water reduces possible quenching effects. Samarium-containing ionic liquids were used to investigate photo-physical properties.[24] The ionic liquid $[C_6MIm][Tf_2N]$ mixed with H_2O or MeCN was used as solvent for samarium containing ionic liquids. Metal-containing ionic liquids with the formula $[C_6MIm][Sm(X)_4]$ (X = tta, nta, hfa) and $[C_6MIm][Sm(X)_3]$ (X = dpa) with different β-diketonate complexes were used. The ionic liquid $[C_6MIm][Tf_2N]$ has been proven to significantly increase the photostability of samarium(III) β-diketonate complexes. A range of crystal structures were reported with tetrakis β-diketonates and the cation $[C_6MIm]^+$.

Prodius *et al.* introduced low-melting, dysprosium-containing ionic liquids with the formula $([Dy(R\text{-}ImCH_2COO)_3(H_2O))_2](Tf_2N)_3)_n$ (R = methyl, ethyl).[25] The melting point of this material was 74°C for the methyl functionalised IL and 87°C for the ethyl-functionalised IL with decomposition temperatures around 240°C. Single crystal structures of these complexes, dysprosium and the carboxylic imidazolium functionality were characterised. The magnetic properties of these compounds were investigated and single ion magnet behaviour at low temperatures was observed.

A series of eleven new rare-earth-containing ionic liquids based on $[La(NO_3)_6]^{3-}$ were reported by Ji *et al.*[26] The ionic liquids have the composition $([C_nMim]_3[La(NO_3)_6]$ (n = 1, 2, 4, 6, 8, 12, 14, 16, 18). These ILs are water-free, which avoids issues with luminescence quenching. These 1-alkyl-3-methylimidazolium hexanitratolanthanates(III) are water stable. The crystal structure of $[C_1Mim]_3[La(NO_3)_6]$ has been described in this report. A $[P_{666\,14}]_3GdCl_6$ has been mentioned earlier in the literature; however, no further characterisation has been reported so far.[27]

Here, we report on a series of phosphonium hexachlorolanthanate ionic liquids with the formulas $([P_{666\,14}]_3[RECl_6]$ (RE = La, Ce, Pr, Nd, Sm, Eu, Gd, Tb, Dy, Ho, Er, Tm,Yb, Lu, Y, Sc). The synthesis, the physical properties, DSC, TGA, UV-Vis, FT-IR, the luminescence and magnetic properties of the complexes are reported and discussed. The lanthanide speciation of the liquid state samples has also been investigated using EXAFS. Analogous solid-state samples with the cations $[P_{4444}]^+$ as well as some selected samples with $[P_{4448}]^+$ have been synthesised and some of the properties have been characterised for comparison.

Results and discussion

A general synthetic scheme for the rare-earth-containing ionic liquids is shown in Scheme 1. The phosphonium chloride ionic liquids and salts were obtained from Cytec Industries. The synthesis of these lanthanide-containing ionic liquids is straightforward and can be done using two synthetic pathways, A or B, depending on whether the used rare-earth chloride salt is hydrated or anhydrous. For pathway A, three equivalents of the phosphonium salts were reacted with one equivalent of the respective hydrated rare-earth salt. Three equivalents of the respective phosphonium chlorides, $[P_{666\,14}]Cl$, $[P_{4444}]Cl$ and $[P_{4448}]Cl$ were dissolved in ethanol. The hydrated rare-earth chloride salts were dissolved in ethanol as well. Both solutions were mixed in a round bottom flask and stirred at room temperature for 1-2 hours. Ethanol was then carefully removed using a rotary evaporator at 80°C. The compounds were then dried overnight under high vacuum at 130°C. The stoichiometry used is 1 : 3 with rare-earth (III) chloride : phosphonium chloride salts.

A. $3[P_{666\,14}]Cl + RECl_3 \rightarrow [P_{666\,14}]_3[RECl_6]$

B. $3[P_{666\,14}]Cl + RECl_3{\cdot}6H_2O \rightarrow [P_{666\,14}]_3[RECl_6] + 6H_2O$

Scheme 1: General pathways A and B for the synthesis of liquid rare-earth. Where RE = La, Ce, Pr, Nd, Sm, Eu, Gd, Tb, Dy, Ho, Er, Tm, Yb, Lu, Y, Sc.

The general formula can be given as $[PR_4]_3[LnCl_6]$ (R = alkyl), with $[P_{666\,14}]Cl$, $[P_{4448}]Cl$ and $[P_{4444}]Cl$ used. It was found that the compounds $[P_{666\,14}]_3[RECl_6]$ (with RE = La, Ce, Pr, Nd, Sm, Eu, Gd, Tm, Tb, Dy, Ho, Er, Yb, Lu, Y, Sc) all result in liquids at room temperature, $[P_{4448}]_3[RECl_6]$ give liquids, supercooled liquids and solids at room temperature and $[P_{4444}]_3[RECl_6]$ results in all solid compounds.

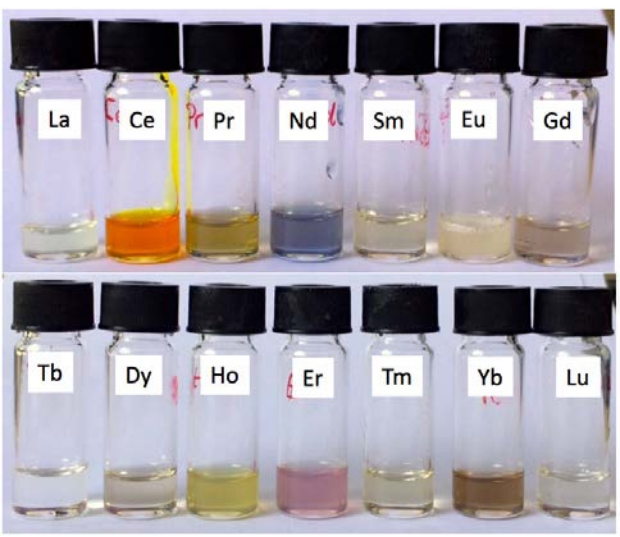

Figure 1. Samples of the room-temperature liquid rare-earth series $[P_{666\,14}]_3[LnCl_6]$ (Ln = La, Ce, Pr, Nd, Sm, Eu, Gd, Tb, Dy, Ho, Er, Tm, Yb, Lu).

Since the hydrated rare-earth chlorides are known to form undesired by-products such as oxochlorides, the first attempts to synthesise the RE series were done with anhydrous rare-earth chlorides (pathway B). In this case, well dried ionic liquid $[P_{666\,14}]Cl$ was added in a glovebox under nitrogen atmosphere to the RE chlorides. The sealed samples were then stirred at around 80°C. The obtained samples were found to be identical with well-dried samples synthesised by pathway A. Synthetic pathway B was found not to be suitable for the samples $[P_{666\,14}]_3[LnCl_6]$ (Ln = La, Ce, Eu and Tm).

Physical Properties. The melting points of these compounds were determined by Differential Scanning Calorimetry (DSC), and were found to be in the range of 43 to 103°C for the $[P_{4444}]_3[RECl_6]$ series, and between -58 and -40°C for the series $[P_{666\,14}]_3[RECl_6]$ (with RE = Ce, Pr, Nd, Sm, Eu, Gd, Tb, Dy, Ho, Er, Tm, Yb, Lu, Y, Sc). The lanthanum compounds is an exception in the series with a melting point of -1.6°C. Therefore, all of the RE compounds containing the $[P_{666\,14}]^+$ cations are liquids at RT; since most of the compounds with the $[P_{4444}]^+$ cations have melting points < 100°C, these could also be considered as ionic liquids. Some selected compounds with the asymmetric $[P_{4448}]^+$ cation have been synthesised as well and show rather irregular behaviour and trends – the melting points for the lighter lanthanides are only slightly lower than for the ones with $[P_{4444}]^+$ cations, but upon cooling, these compounds behave as super-cooled liquids with rather low crystallisation temperatures ranging between 12 and 18°C. The heavier lanthanides with the $[P_{4448}]^+$ cation have relatively low melting points ranging from -6 to -48°C. Details of the melting points and glass transitions are shown in Table 1. The liquid phosphonium rare-earth complexes show high thermal stability with decomposition temperatures between 340 and 380°C.

Table 1: Melting points and glass transition temperatures for the series $[PR_4]_3[RECl_6]$ (Ln = La, Ce, Pr, Nd, Sm, Eu, Gd, Tb, Dy, Ho, Er, Tm, Yb, Lu, Y and Sc).

RE metal	$[P_{4444}]^+$ / °C	$[P_{4448}]^+$ / °C	$[P_{666\,14}]^+$ / °C
La	102.8 (m.p.)	-	-1.6 (m.p.)
Ce	62.2 (m.p.)	-25.2 (T_g) 12.3 (T_c); 53.2(m.p.)	-58.2 (m.p.)
Pr	95.8 (m.p.)	-	-40.9 (m.p.)
Nd	65.3 (m.p.)	-25.5 (T_g); 15.3 (T_c); 46.4 (m.p.)	-45.5 (m.p.)
Sm	58.8 (m.p.)	-23.1 (T_g); 17.9 (T_c); 47.3 (m.p.)	-44.9 (m.p.)
Eu	55.3 (m.p.)	-44 (T_g); -21 (m.p.)	-- --
Gd	52.4 (m.p.)	-	-58.8 (m.p.)
Tb	51.6 (m.p.)	-25.1 (T_g)	-49.1 (m.p.)
Dy	42.9 (m.p.)	-31.4 (T_g); -6.1 (T_c); 3.3 (m.p.)	-47.7 (m.p.)
Ho	48.8 (m.p.)	-	-42.1 (m.p.)
Er	51.3 (m.p.)	-67.9 (T_g); -48 (m.p.)	-40.4 (m.p.)
Tm	65.6 (m.p.)	-	-41.1 (m.p.)
Yb	51.8 (m.p.)	-	-41.4 (m.p.)
Lu	46.9 (m.p.)	-	-43.1 (m.p.)
Y	69.5 (m.p.)	-	-43.2 (m.p.)
Sc	57.3 (m.p.)	-	-62.8 (m.p.)

Crystal structure

None of the compounds with $[P_{666\,14}]^+$ cations crystallises; therefore, suitable crystals for structure determination were obtained from the room temperature solids with a symmetric cation, $[P_{4444}]^+$. However, obtaining a crystal structure with reasonable quality turned out to be difficult even with these symmetric cations. Crystals of $[P_{4444}]_3[EuCl_6]$ were obtained by slowly cooling a melt from 80°C in a sealed ampoule to room temperature. Due to their hygroscopic nature, the crystals were collected in a glovebox under argon and sealed in quartz capillaries for the X-ray measurement. The crystal structure contains, as expected, $[EuCl_6]^{3-}$ anions which are each surrounded by 3 crystallographically independent $[P_{4444}]^+$ cations (see Figure 2). One of the alkyl chains on the P2 cation is disordered. All alkyl chains of the phosphonium cations show large temperature factors and have not been refined anisotropically. The packing in the large cell (space group $P4_12_12_1$; a = 16.5192(6) Å; b = 16.5192(6) Å; c = 46.471(3) Å) is shown in Figure 3.

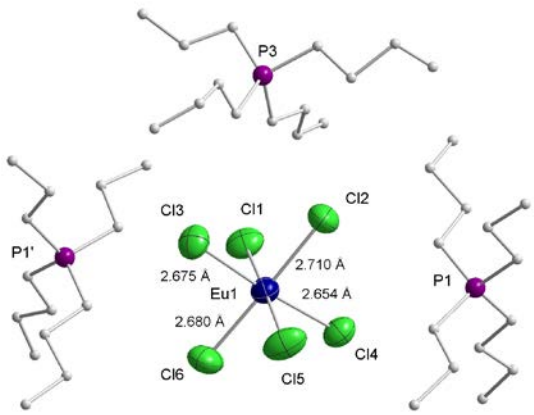

Figure 2. Packing in the unit cell of $[P_{4444}]_3[EuCl_6]$.

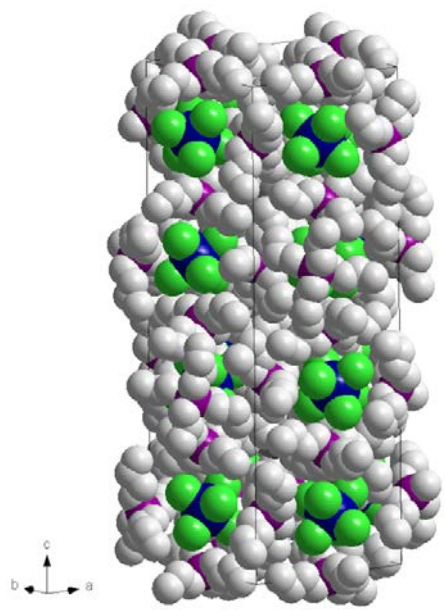

Figure 3. Packing in the large unit cell of $[P_{4444}]_3[EuCl_6]$.

EXAFS for the liquid state samples

Three ionic liquid samples were selected and investigated by means of X-ray Absorption Spectroscopy (XAS). These samples consist of $[P_{666\,14}]^+$ cations and $[LnCl_6]^{3-}$ anions (where Ln = Nd, Eu and Dy, respectively). The EXAFS-spectra and corresponding Fourier-transform (FT) signal for these samples are given in Figures 4-6. The EXAFS data are summarised in Table 2.

$[P_{666\,14}]_3[NdCl_6]$. The FT signal for the Nd sample (Figure 4, right) is dominated by a single shell at R + Δ = 2.4 Å (corresponding to a real distance R = 2.70 Å), and a smaller peak at R

+ Δ = 4.8 Å (corresponding to a real distance R = 5.39 Å) can also be observed. The single shell at 2.70 Å represents the six chloride ligands and the smaller band at double this distance is the multiple scattering signal for the same ligands.

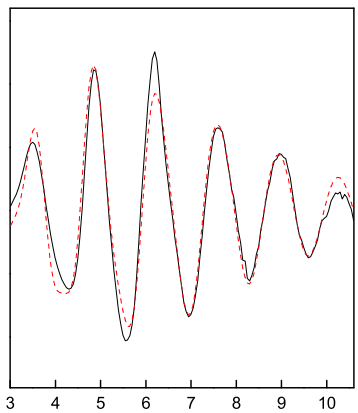

Figure 4. Nd L_{III} edge EXAFS spectrum (left) and corresponding Fourier transform (right) of the ionic liquid $[P_{666\,14}]_3[NdCl_6]$.

$[P_{666\,14}]_3[EuCl_6]$. The EXAFS spectrum and the corresponding FT signal (Figure 5) for this sample look quite similar to those of the Nd sample. The FT signal is also dominated by a single shell at R + Δ = 2.3 Å (corresponding to a real distance R = 2.66 Å), and a smaller peak at R + Δ = 4.6 Å (corresponding to a real distance R = 5.33 Å) can also be observed. The single shell at 2.66 Å again represents the six chloride ligands and the smaller band at double this distance is the multiple scattering signal for the same ligands.

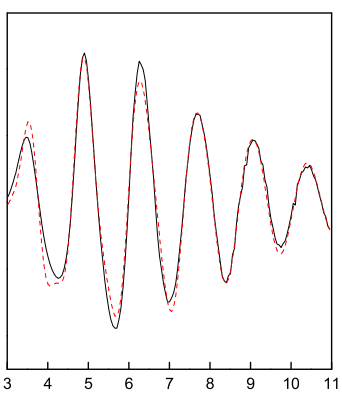

Figure 5. Eu L_{III} edge EXAFS spectrum (left) and corresponding Fourier transform (right) of the ionic liquid $[P_{666\,14}]_3[EuCl_6]$.

$[P_{666\,14}]_3[DyCl_6]$. The EXAFS-spectrum and corresponding FT signal for this sample are given in Figure 6 and again are very comparable to the features in Figures 4 and 5. The only difference is a slightly larger k-range for the heavier lanthanides, as the energy separation between the L_{III} and L_{II} edges becomes larger with increasing Z. For the Dy sample the FT is also dominated by a single shell at R + Δ = 2.2 Å (corresponding to a real distance R = 2.65 Å), representing the six chloride ligands, and the smaller peak at R + Δ = 4.4 Å (corresponding to a real distance R = 5.29 Å) from the multiple scattering signal for the same ligands.

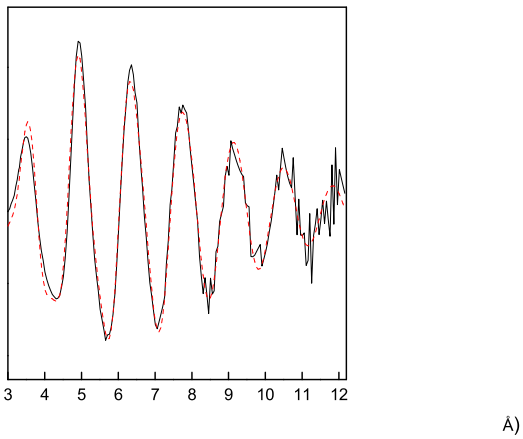

Figure 6. Dy L_{III} edge EXAFS spectrum (left) and corresponding Fourier transform (right) of the ionic liquid $[P_{666\,14}]_3[DyCl_6]$.

Table 2. EXAFS structural parameters for $[P_{666\,14}]_3[LnCl_6]$ (Ln = Nd, Eu, Dy)

sample	scattering path	R (Å)	N	σ^2 (Å^2)
$[P_{666\,14}]_3[NdCl_6]^b$	Nd···Cl single	2.696(3)	6.1(3)	0.0091(6)
	Nd···Cl multiple	5.393[a]		0.0182[a]
$[P_{666\,14}]_3[EuCl_6]^c$	Eu···Cl single	2.664(2)	6.7(2)	0.0089(4)
	Eu···Cl multiple	5.327[a]		0.0179[a]
$[P_{666\,14}]_3[DyCl_6]^d$	Dy···Cl single	2.647(2)	6.4(2)	0.0087(3)
	Dy···Cl multiple	5.293[a]		0.0173[a]

[a] Values fixed at double the single path values

[b] ΔE = –0.1(5) eV; weighted *F*-factor = 0.29

[c] ΔE = –0.2(3) eV; weighted *F*-factor = 0.21

[d] ΔE = 1.0(3) eV; weighted *F*-factor = 0.23

The EXAFS measurements confirm the hexa-coordination of the lanthanide ions by six chloride ligands in the liquid state. Furthermore, these measurements show that the Ln···Cl distance decreases with decreasing lanthanide ionic radius: 2.70 Å (270 pm) for Nd^{3+} (ionic radius = 98.3 pm for the six-coordinated trivalent ion), 2.66 Å (266 pm) for Eu^{3+} (ionic radius = 94.7 pm for the six-coordinated trivalent ion) and 2.65 Å (265 pm) for Dy^{3+} (ionic radius = 91.2 pm for the six-coordinated trivalent ion). The increasing charge density leads to a stronger attraction between the lanthanide ion and the chloride ligands, resulting in a shorter Ln···Cl distance.

Luminescence properties

Lanthanides have intrinsic luminescence properties due to their f-f transitions. Some of the liquid compounds that show lumi-

nescence have been investigated. Terbium and europium show visible-light luminescence (see Figure 7). Furthermore, samarium and dysprosium (see supporting info) and the NIR luminescence of the neodymium and erbium compounds have been measured.

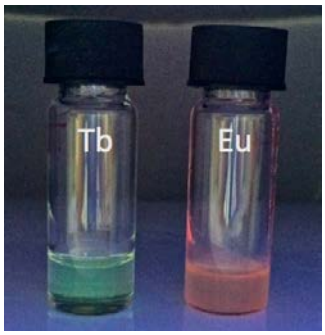

Figure 7. Visible light luminescence of $[P_{666\,14}]_3[TbCl_6]$ (left) and $[P_{666\,14}]_3[EuCl_6]$ (right) upon UV excitation (332 nm).

$[P_{666\,14}]_3[EuCl_6]$. Upon excitation at 393.7 nm (25400 cm^{-1}), in the $^5L_6 \leftarrow {}^7F_0$ transition, the sample shows typical narrow Eu^{3+} emission peaks (see Figure 8). The peaks labelled j-n have been assigned to the corresponding electronic transitions in Table 3.
The sample could also be excited at 339.6 nm (29446 cm^{-1}) giving rise to the same Eu^{3+} peaks as when excited at 393.7 nm. No significant difference in intensity was observed.
Monitoring the emission of the sample at 611.8 nm (16345 cm^{-1}, $^5D_0 \rightarrow {}^7F_2$ transition), the excitation wavelength was varied between 250 and 500 nm to record an excitation spectrum. In the spectrum a broad band with a maximum at 339.6 nm (29446 cm^{-1}) is visible. All other peaks in the spectrum can be assigned to transitions within the Eu^{3+} ion's 4f shell. The peaks labelled a-i have been assigned to the corresponding transitions in Table 3.
Upon excitation at 355 nm with a pulsed light source, the emission at 611.8 nm shows a mono-exponential decay profile, corresponding to a luminescence decay time of 1095 µs or 1.095 ms (Figure S9, Supporting Information).
$[P_{666\,14}]_3[TbCl_6]$. Upon excitation at 378.1 nm (26448 cm^{-1}), in the $^5G_6$, $^5D_3 \leftarrow {}^7F_6$ transitions, the sample shows typical narrow Tb^{3+} emission peaks (Figure 9). The peaks labelled e-h have been assigned to the corresponding electronic transitions in Table 3. The sample was also excited at 272.5 nm (36697 cm^{-1}) giving rise to typical Tb^{3+} peaks, but more intensive then when excited at 378.1 nm. Monitoring the emission of the sample at 548.2 nm (18242 cm^{-1}, $^5D_4 \rightarrow {}^7F_5$ transition), the excitation wavelength was varied between 250 and 500 nm to record an excitation spectrum (Figure 9). In the spectrum a broad band with a maximum at 272.5 nm (36697 cm^{-1}) is visible. All other peaks in the spectrum can be assigned to transitions within the Tb^{3+} ion's 4f shell. The peaks labelled a-d have been assigned to the corresponding transitions in Table 3.

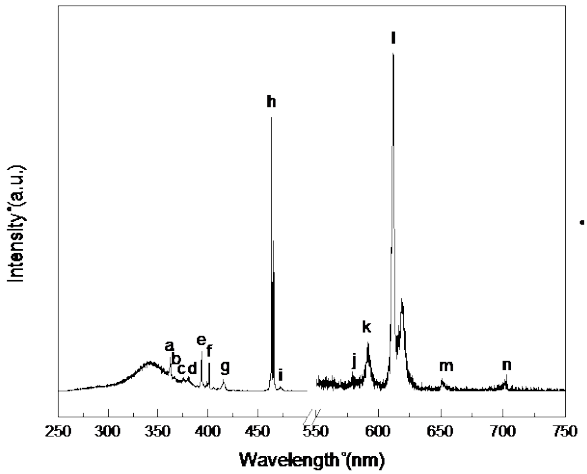

Figure 8: Excitation and emission spectrum of $[P_{666\,14}]_3[EuCl_6]$; excitation monitored at 611.8 nm and emission excited at 339.6 nm (corrected for detector sensitivity).

Upon excitation at 355.0 nm with a pulsed light source, the emission at 548.2 nm shows a mono-exponential decay profile. The luminescence decay time is calculated as 692 µs or 0.692 ms (Figure S24, Supporting Information).

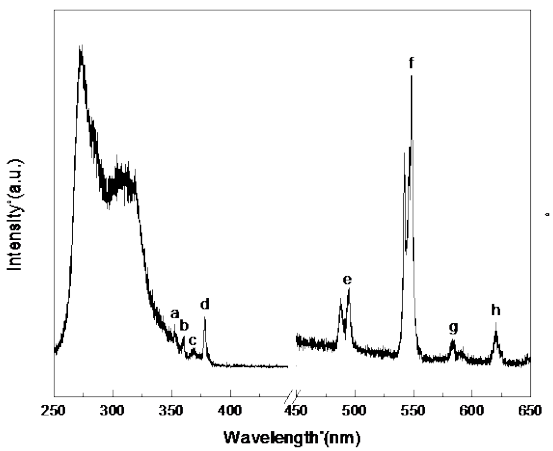

Figure 9: Excitation and emission spectrum of $[P_{666\,14}]_3[TbCl_6]$; excitation monitored at 548.2 nm and emission excited at 378.1 nm (corrected for detector sensitivity).

$[P_{666\,14}]_3[NdCl_6]$. Upon excitation at 586.0 nm nm (17065 cm^{-1}), in the $^2G_{7/2}$, $^4G_{5/2} \leftarrow {}^4I_{9/2}$ transition, the sample shows typical narrow Nd^{3+} emission peaks (Fig. 10). The peaks labelled a-c have been assigned to the corresponding electronic transitions in Table 4. Monitoring the emission of the sample at 1064.0 nm (9399 cm^{-1}, $^4F_{3/2} \rightarrow {}^4I_{11/2}$ transition), the excitation wavelength was varied between 250 and 850 nm to record an excitation spectrum.

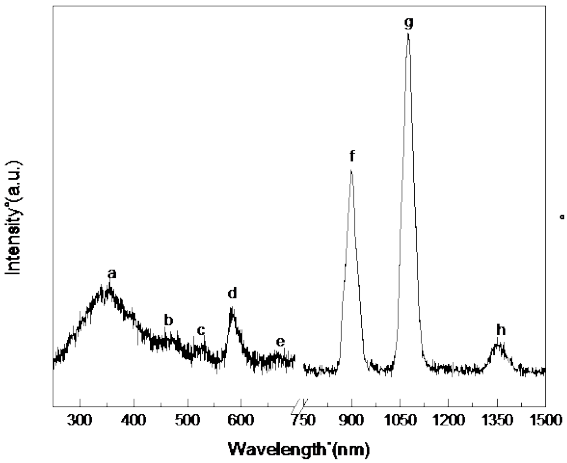

Figure 10: Excitation and emission spectrum of $[P_{666\ 14}]_3[NdCl_6]$; excitation monitored at 1064.0 nm and emission excited at 393.7 nm (corrected for detector sensitivity).

All the peaks in the spectrum can be assigned to transitions within the Nd^{3+} ion's 4f shell. The peaks labelled a-e have been assigned to the corresponding transitions in Table 4. Upon excitation at 355.0 nm with a pulsed light source, the emission at 1064.0 nm shows a mono-exponential decay profile. The luminescence decay profile is given in Figure S62 (Supporting Information). The luminescence decay time was calculated as 2470 ns or 2.470 µs, which is rather long for Nd^{3+} in an organic compound. In comparison, Nd^{3+} in a terephthalate MOF has been reported to have a luminescence decay time of only 0.43 µs.[28] This much shorter decay time can be explained by the coordinated water in this MOF, bringing O-H vibrations in very close proximity of the Nd^{3+} ion and causing strong quenching of the luminescence and shortening of the decay time. The hexachloride coordination in the ionic liquid sample provides much improved protection against quenching influences, hence the longer luminescence decay time.

$[P_{666\ 14}]_3[ErCl_6]$. Upon excitation at 375.0 nm (26667 cm^{-1}) with a CW diode laser, the sample shows only one narrow emission peak of Er^{3+} (Figure 11). This peak, with a maximum at 1543.0 nm (6481 cm^{-1}), can be assigned to the $^4I_{13/2} \rightarrow {}^4I_{15/2}$ transition. Monitoring the emission of the sample at 1543.0 nm (6481 cm^{-1}, $^4I_{13/2} \rightarrow {}^4I_{15/2}$ transition) the excitation wavelength was varied between 250 and 700 nm to record an excitation spectrum. Four peaks are visible in the spectrum and can be assigned to transitions within the Er^{3+} ion's 4f shell.

Table 3. Assignment of the 4f-4f transitions in the excitation and emission spectra of samples $[P_{666\ 14}]_3[EuCl_6]$ and $[P_{666\ 14}]_3[TbCl_6]$.

	Excitation					Emission			
	Wavelength (nm)	Energy (cm^{-1})	Transition			Wavelength (nm)	Energy (cm^{-1})	Transition	
				$[P_{66614}]_3[EuCl_6]$					
a	362.4	27594	$^5D_4$	$\leftarrow {}^7F_0$	j	579.3	17262	$^5D_0 \rightarrow$	$^7F_0$
b	367.0	27248	$^5D_4$	$\leftarrow {}^7F_1$	k	591.8	16898		$^7F_1$
c	374.7	26688	$^5G_{6,4}$	$\leftarrow {}^7F_0$	l	611.8	16345		$^7F_2$
d	379.4	26357	$^5G_{6,5,3}$	$\leftarrow {}^7F_1$	m	650.7	15368		$^7F_3$
e	393.7	25400	$^5L_6$	$\leftarrow {}^7F_0$	n	701.6	14253		$^7F_4$
f	401.5	24907	$^5L_6$	$\leftarrow {}^7F_1$					
g	415.8	24050	$^5D_3$	$\leftarrow {}^7F_1$					
h	464.1	21547	$^5D_2$	$\leftarrow {}^7F_0$					
i	472.7	21155	$^5D_2$	$\leftarrow {}^7F_1$					
				$[P_{66614}]_3[TbCl_6]$					
a	352.5	28369	$^5L_9$	$\leftarrow {}^7F_6$	e	495.0	20202	$^5D_4 \rightarrow$	$^7F_6$
b	360.6	27732	$^5G_5$		f	548.2	18242		$^7F_5$
c	369.8	27042	$^5L_{10}$		g	583.4	17141		$^7F_4$
d	378.1	26448	$^5G_6$, $^5D_3$		h	620.1	16126		$^7F_3$

Table 4. Assignment of the 4f-4f transitions in the excitation and emission spectra of samples $[P_{666\,14}]_3[NdCl_6]$ and $[P_{666\,14}]_3[ErCl_6]$.

	Excitation					Emission			
	Wave-length (nm)	Energy (cm^{-1})	Transition			Wavelength (nm)	Energy (cm^{-1})	Transition	
			$[P_{66614}]_3[NdCl_6]$						
a	356.0	28090	$^2L_{15/2}$, $^4D_{1/2}$, $^2I_{11/2}$, $^4D_{5/2}$, $^4D_{3/2}$	$\leftarrow {}^4I_{9/2}$	f	897.0	11148	$^4F_{3/2} \rightarrow$	$^4I_{9/2}$
b	467.0	21413	$^4G_{11/2}$, $^2D_{3/2}$, $^2P_{3/2}$, $^2G_{9/2}$, $^2K_{15/2}$		g	1064.0	9399		$^4I_{11/2}$
c	533.0	18762	$^4G_{9/2}$, $^4G_{7/2}$, $^2K1_{3/2}$		h	1351.0	7402		$^4I_{13/2}$
d	586.0	17065	$^2G_{7/2}$, $^4G_{5/2}$						
e	681.0	14684	$^4F_{9/2}$						
			$[P_{66614}]_3[ErCl_6]$						
a	382.0	26178	$^4G_{11/2}$	$\leftarrow {}^4I_{15/2}$	e	1543.0	6481	$^4I_{13/2} \rightarrow$	$^4I_{15/2}$
b	465.0	21505	$^4F_{3/2}$, $^4F_{5/2}$, $^4F_{7/2}$						
c	525.0	19048	$^4H_{11/2}$						
d	655.0	15267	$^4F_{9/2}$						

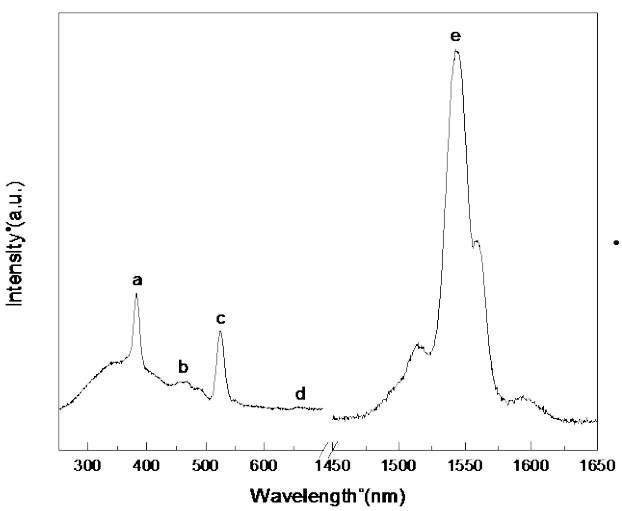

Figure 11: Excitation and emission spectrum of $[P_{666\,14}]_3[ErCl_6]$; excitation monitored at 1543.0 nm and emission excited at 375.0 nm (corrected for detector sensitivity).

The peaks labelled a-d have been assigned to the corresponding transitions in Table 4. Upon excitation at 355.0 nm with a pulsed light source, the emission at 1543.0 nm shows a mono-exponential decay profile. The luminescence decay profile is given in Fig. S71 (Supporting Information). The luminescence decay time was calculated as 2725 ns or 2.725 µs.

Magnetic Measurements. The results of the temperature dependant magnetisation measurements are plotted in Figure 12 as the product of $\chi_M T$ for the Nd, Er, Tb, Dy, Gd and Ho samples. The small variation for the background contribution for different sample capsules and mounting straws and heat contraction/expansion of the mounting straw moving the sample slightly off-centre during temperature scans contributes an uncertainty of around 5% to the magnetic moment. This is shown by the error bars in Figure S73 in the Supplement. All the samples displayed simple paramagnetic behaviour over the temperature range studied and returned constant $\chi_M T$ values, shown in Table 5. Constant $\chi_M T$ values are expected, given the large distance between the metal ions. The Curie and Weiss constants for the different samples shown in Table S35 (Supplement) were obtained by fitting to the Curie-Weiss law

$$X = \frac{C}{T - \theta} \qquad (1)$$

where C is the Curie constant, T is the temperature in kelvin and θ is the Weiss constant, see Figure S73.

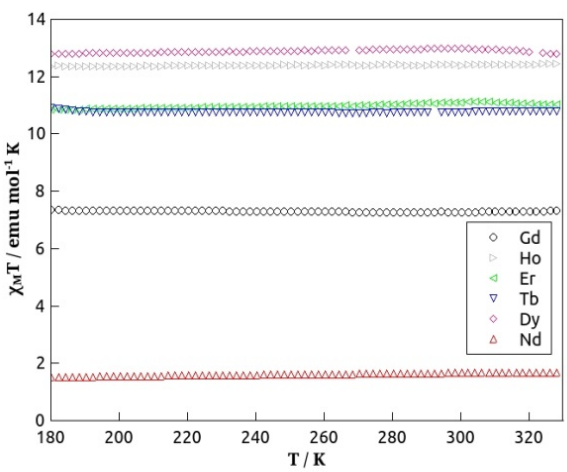

Figure 12. Plot of $\chi_M T$ vs T for Er, Tb, Dy and Nd samples in the temperature range 180K-330K, collected on heating with an applied field of 500 Oe.

The effective magnetic moments are consistent with those in the literature for the observed values of the lanthanide ions, within the range of experimental uncertainty. It should be noted that the Weiss temperatures are small enough that they can be taken to be zero within the experimental uncertainties. The Weiss temperature for the Nd sample is significantly larger than that for the other samples. This is due to the increased uncertainty in the measurement resulting from the much smaller magnetic response.

Table 5. Experimental and literature effective magnetic moments, and $\chi_M T$ values for Dy, Nd, Er, Tb, Ho and Gd samples.

RE metal	μ_{eff} Exp / μ_B	μ_{eff} Lit / μ_B[29]	$\chi_M T$ / emu·mol^{-1}·K^{-1}
Dy	10.2 ± 0.9	10.4 - 10.7	12.9 ± 0.6
Nd	3.9 ± 0.4	3.5 - 3.6	1.6 ± 0.1
Er	9.5 ± 0.9	9.4 - 9.6	11.0 ± 0.6
Tb	9.3 ± 0.8	9.5 - 9.8	10.8 ± 0.5
Ho	10.0 ± 0.9	10.4 - 10.7	12.4 ± 0.6
Gd	7.7 ± 0.7	7.9 - 8.0	7.3 ± 0.4

The data for the Nd sample can however be convincingly fit with the Weiss temperature equal to zero. The Eu and Sm data were omitted completely as the measured magnetic response was too small to obtain a reliable effective magnetic moment, which from literature is observed to be in the ranges 3.3-3.5 B.M and 1.4-1.7 B.M. respectively.

Electrochemical measurements. The electrochemical behaviour of $[P_{666\ 14}]_3[LnCl_6]$ ionic liquids were tested using cyclic voltammetry. A cyclic voltammogram of $[P_{666\ 14}]_3[LaCl_6]$ is presented in Fig. 13 as an example.

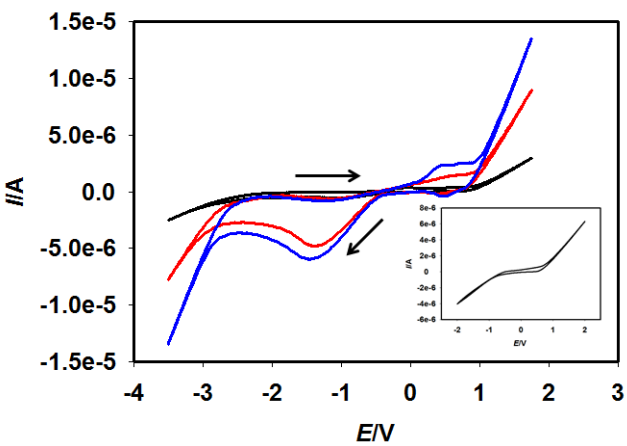

Figure 13. Cyclic voltammograms of $[P_{666\ 14}]_3[LaCl_6]$ ionic liquid at various temperatures; black - 110 °C, red - 120 °C and blue - 130 °C on Pt as the working electrode *vs.* Ag/Ag^+ as reference electrode.

Addition of $LaCl_3$ to $[P_{666\ 14}]Cl$ altered its electrochemical behaviour (inset in Figure 13 shows cyclic voltammetry of $[P_{666\ 14}]Cl$), thereby confirming the change in the anionic speciation of $[P_{666\ 14}]_3[LaCl_6]$ system. To reduce viscosity, voltammetric measurements were carried out at 110 °C and further increased to 120°C and 130°C. On the forward scan (towards the cathodic direction), a broad reduction peak around -1.5 V was observed and on the reverse scan (towards anodic direction), an oxidation peak around 0.6 V appeared. When the scan direction was changed (anodic first), no peak around 0.6 V was observed which enabled the assignment of this peak to the oxidation of the reduced species at -1.5 V. These redox peaks became more pronounced with increment in current when the temperature of the electrolyte was increased; increase in current may be accounted for by reduction of the viscosity and thereby an increasing of the conductivity and mobility of the ions towards the electrodes. Chlorolanthanates unlike chloroaluminate ILs[30] did not show conventional electrodeposition of the La(0) and stripping peaks in the cyclic voltammogram. Although in non-halometallate ionic liquid electrolytes[31] reduction of La(III) to La(0) is favoured thermodynamically, in a chloride rich, chlorometallate environment, existence of La(II) has been reported to be feasible.[32,33] Chloride as a strong complexing ligand probably hinders the electroreduction of the $[LaCl_6]^{3-}$ species, whereas a dicyanamide complex of lanthanum favours electroreduction of lanthanum to its elemental form as reported in the literature.[34] Electrodeposition of metallic lanthanum from N-methyl-N-propylpiperidinium bis(trifluoromethylsulfonyl)-imide ionic liquid has also been reported.[35] All the current experiments were carried out in argon atmosphere inside a glove box, which eludes the possibility of interference by oxygen and moisture. Therefore, the redox peaks could be attributed to the reduction of La(III) to La(II) and then oxidation back to La(III). The oxidation process may be partial since the current area for the reduction peak is much larger than the area for the oxidation peak. Electrodeposition experiments were carried out using chronoamperometry by holding the potential at -1.5 V for 12 h at 150°C. No metallic deposits of La were observed.

Experimental

EXAFS. Nd L_{III} edge (6.028 keV), Eu L_{III} edge (6.997 keV) and Dy L_{III} edge (7.790 keV) Extended X-ray Absorption Fine Structure (EXAFS) spectra of ionic liquid samples at room temperature were collected at the Dutch-Belgian Beamline (DUBBLE) at the European Synchrotron Radiation Facility (ESRF).[36,37] The energy of the X-ray beam was tuned by a double-crystal monochromator operating in fixed-exit mode using a Si(111) crystal pair. A vertically collimating mirror in front of the monochromator and a vertically focusing mirror behind the monochromator, each with Si and Pt coatings, were used to align the beam during energy changes. The samples were measured in transmission mode using a N_2/He filled first ionization chamber and an Ar/He-filled second ionization chamber to allow approximately 10% and 70% absorption respectively. For the liquid samples, custom-made brass sample holders have been designed which allow measurement of very thin samples (less than 1 mm path length), air-tight and Kapton-windowed. The energy calibration was done using Fe foil (7.112 keV). Several scans were collected for each sample to check for reproducibility of the data and were averaged to improve the signal-to-noise ratio.

EXAFS data extraction and data fitting was performed using the programs WinXAS[38], EXAFSPAK[39] and the Artemis suite[40]. Theoretical phase and amplitude functions were calculated using FEFF 8.2[41] using the crystal structure of $[Emim]_3[EuCl_6]$.

Standard deviations on the fitted parameters have been mentioned between brackets. However, it should be noted that these values are most likely an underestimation of the real errors on the obtained values as also other errors have to be taken into account, such as systematic errors and correlation effects, which are much more difficult to

estimate. This means that the real errors can be considerably larger than this standard deviation (which only indicates how much the parameters can vary without degrading the quality of the fit). General errors on coordination numbers of single shells are estimated to be in the order of 10 – 15%. Errors in distances are usually quite small, usually in the order of ± 0.01 Å, as this is something that EXAFS can determine very accurately. Debye-Waller factors σ^2 are strongly correlated with the coordination number in the EXAFS formula, so errors on the Debye-Waller factors can also range between 10 and 25%. A more general idea of the goodness of the fit is given by the "weighted F-factor", a parameter generated by the EXAFSPAK software package[39], representing χ^2 weighted by the magnitude of the data, and typically lying between 0.30 and 0.10 for a reasonable to good fit.

Differential scanning calorimetry (DSC). Thermal profiles of the ionic liquids were obtained using a TA DSC Q2000 model with a TA Refrigerated Cooling System 90 (RCS), with the ILs sealed in a glovebox in TA Tzero alodined pans with hermetic alodined lids. A cooling and heating ramp of 5 °C min^{-1} was used, within the temperature ranging from -150 to 150 °C, and three scans were carried out for each sample.

Thermogravimetric analysis (TGA). The temperature of decomposition was measured using a TA TGA Q5000, at a heating rate of 5 °C min^{-1}. All samples were sealed in the glovebox, in aluminium pans. The onset of the weight loss in each thermogram was used as a measure of the decomposition temperature.

Karl Fischer analysis. The water content of ionic liquids was measured by coulometric Karl Fischer titration using a GRScientific Cou-Lo Aquamax KF Moisture Meter. All samples were dried under high vacuum (60 °C, overnight) and stored in the glovebox prior to the measurements.

DC magnetic susceptibility measurements were preformed using a Quantum Design MPMS DC XL SQUID magnetometer under an applied field of 100 Oe. The magnetization was measured as a function of temperature in the range 180 K – 380 K both on heating and cooling the samples. There was no difference in the results observed. Diamagnetic corrections were calculated from Pascal's constants[42] and applied to all data.

Voltammetric experiments were carried out using 2 gram of ionic liquid in a three-electrode arrangement with platinum (1.6 mm diameter) as the working electrode, a bright platinum coil as the counter electrode in a counter compartment with the same electrolyte as used in the bulk experiment and separated from the bulk solution *via* a glass frit, and all potentials measured with respect to an Ag^+/Ag reference (a silver wire immersed in 0.01 M $AgNO_3$ solution in 1-butyl-3-methylimidazolium nitrate, $[C_4mim][NO_3]$) and separated from the bulk solution *via* a glass frit. The *IR*-drop was uncompensated. The platinum working electrode (Pt-BASi, US) was polished using an alumina slurry (Kemet, UK) of decreasing particle size (6–0.1 μm) on soft lapping pads, washed with distilled water, sonicated for 10 min, and dried with compressed air prior to each experiment. Electrodeposition experiments were carried out using a platinum disc of surface area 0.75 cm^2 (Alfa Aesar), the reference and counter electrodes being the same as for the voltammetric experiments. Cyclic voltammograms and potentiostatic deposition experiments were carried out with a PC-controlled Autolab Type III Potentiostat.

Photoluminescence measurements were recorded on an Edinburgh Instruments FLSP920 UV-Vis-NIR spectrofluorimeter, using a 450 W xenon lamp as the steady state excitation source, a Hamamatsu R928P PMT photomultiplier working at -22°C for the visible range and a Hamamatsu R5509-72 photomultiplier operating at -80°C for the NIR range. For the Er^{3+} ionic liquid samples the emission spectra were recorded using either a 100 mW CW diode laser emitting at 375 nm (only for sample $[P_{666\,14}][ErCl_6]$) or a Surelite I laser (450 mJ @1064 nm), operating at a repetition rate of 10 Hz and using the third harmonic (355 nm) as the excitation source.

The time-resolved measurements were performed using the Continuum Surelite I laser (450 mJ @1064 nm), operating at a repetition rate of 10Hz and using the third harmonic (355 nm) as the excitation source, and the photomultiplier detectors mentioned above. For Ce^{3+}, Nd^{3+}, and Er^{3+} samples a MSA card was additionally used to allow recording luminescence lifetimes in the nanosecond range.

Crystallography

The frames were integrated using the Bruker SAINT software package. Using a narrow-frame algorithm. Data were corrected for absorption effects using the numerical method with SADABS. A suitable crystal of $[P_{666\,14}][EuCl_6]$ was selected and measured on a four-circle diffractometer Kappa APEX II (Bruker AXS) with CCD detector and graphite-monochromated Mo Kα radiation. The crystal was kept at 200.15 K during data collection. Using Olex2[43], the structure was solved by direct methods using the ShelXS structure solution program and refined by full-matrix least-squares on F2 using the ShelXL program package.[44] Non-hydrogen atoms were anisotropically refined and the hydrogen atoms in the riding mode and isotropic temperature factors fixed at 1.2 times U(eq) of the parent atoms (1.5 times for methyl groups and the hydroxyl group).

CCDC-1446352 contains the supplementary crystallographic data for this paper and can be obtained free of charge via www.ccdc.cam.ac.uk/conts/retrieving.html (or from the Cambridge Crystallographic Data Centre, 12, Union Road, Cambridge CB2 1EZ, UK; fax: +44-1223-336033; or deposit@ccdc.cam.ac.uk).

Crystal Data for $[P_{666\,14}][EuCl_6]$, ($C_{48}H_{108}P_3Cl_6Eu$) (M =1142.91 g/mol): tetragonal, space group $P4_12_12$ (no. 92), a = 16.5192(6) Å, c = 46.471(3) Å, V = 12681.2(10) $Å^3$, Z = 8, T = 200 K, μ(MoKα) = 1.345 mm^{-1}, $Dcalc$ = 1.197 g/cm^3, 54427 reflections measured (2.62° ≤ 2Θ ≤ 40.32°), 6040 unique (R_{int} = 0.0871, R_{sigma} = 0.0517) which were used in all calculations. The final R_1 was 0.1271 (>2sigma(I)) and wR_2 was 0.2863 (all data).

Synthesis

The rare earth chlorides were purchased from Sigma-Aldrich. Two different synthetic pathways can be used - for **pathway A**, 3 mmol of the respective phosphonium chlorides, $[P_{666\,14}]Cl$, $[P_{4444}]Cl$ and $[P_{4448}]Cl$ were reacted with 1 mmol of the respective anhydrous rare-earth salt. The mixture was prepared in a glove-box under nitrogen and sealed in glass vials with a magnetic stirring bar. The reaction mixtures were heated to 80°C for 3 h under stirring. For **pathway B**, the cheaper hydrated rare-earth salts were used. 3 mmol of the respective phosphonium chlorides, $[P_{666\,14}]Cl$, $[P_{4444}]Cl$ and $[P_{4448}]Cl$ were dissolved in ethanol. The hydrated rare-earth chloride salts were dissolved in ethanol as well. Both solutions were mixed in a round bottom flask and stirred at room temperature for 3 hours. Ethanol was then carefully removed using a rotary evaporator at 80°C. The compounds were then dried overnight under high vacuum at 130°C. All compounds were characterised by CHN analysis; a table with the calculated and obtained values can be found in the Supporting Information (Table S34). Karl-Fischer titrations to determine the water content of the samples showed values of < 20 ppm for all samples; however, the samples were found to be hygroscopic (the smaller the phosphonium cations, the more hygroscopic) and rapidly absorb water when exposed to air.

Conclusions

We have synthesised and characterised ionic liquid chlorometallate complexes using the $[P_{666\,14}]^+$ cation for the whole rare earth series with melting temperatures below 0°C. The crystal structure of $[P_{4444}][EuCl_6]$ as an analogue to the liquid samples was determined and shows hydrogen bonding of the $[EuCl_6]^{3-}$ with the α-protons of three surrounding phosphonium cations. Due to the long alkyl chains on the cations, the quality of the crystal structure determination is limited, but the crystallographic model is good enough to confirm the

expected octahedral coordination and cation / anion interactions.

The EXAFS spectra of three hexachloro lanthanate ionic liquids with Ln = Eu, Nd and Dy, could be satisfactorily fitted with one single scattering Ln···Cl shell and one multiple scattering shell with double the distance of the single shell. Within the EXAFS error margins, the coordination number is equal to that of the reference materials, *i.e.* six. The EXAFS measurements show that the Ln···Cl distance decreases with decreasing lanthanide ionic radius: 270 pm for Nd^{3+} (ionic radius = 98.3 pm for the six-coordinated trivalent ion), 266 pm for Eu^{3+} (ionic radius = 94.7 pm for the six-coordinated trivalent ion) and 265 pm for Dy^{3+} (ionic radius = 91.2 pm for the six-coordinated trivalent ion). The increasing charge density leads to a stronger attraction between the lanthanide ion and the chloride ligands, resulting in a shorter Ln···Cl distance.

The luminescence spectra for Tb and Eu show visible light emissions, whereas NIR luminescence was observed for Nd and Er. Relatively long luminescence lifetimes were found for the NIR emitter (Nd: 2.470 µs and Er: 2.725 µs).

The magnetic susceptibility measurements showed all of the measured samples (Dy, Tb, Gd, Nd, Er, and Ho) to be paramagnetic with effective magnetic moments that are all within the expected range for trivalent ions of the respective rare earth elements.

Supporting Information

Electronic Supplementary Information (ESI) available: Electronic Supplementary Information (ESI) available: excitation and emission spectra, luminescence decay traces, CHN results.

ACKNOWLEDGMENT

P.N. and S.F. thank the Royal Society for a Research Grant (RG130739). We thank Seagate Technology (Ireland) for their financial support to establish ANSIN (www.ansin.eu). R.V.D. thanks the Hercules Foundation (project AUGE/09/024 “Advanced Luminescence Setup”) for funding. A. M. K. acknowledges Ghent University’s Special Research Fund (BOF) for a Postdoctoral Mandate (project BOF15/PDO/091). We thank the FWO-Vlaanderen and the Netherlands Organisation for Scientific Research (NWO) for providing beam time at the Dutch–Belgian Beamline (DUBBLE, BM26A, ESRF). Matthias Groh and Alexander Wolff from TU Dresden are acknowledged for help with crystal data collection. The authors would like to thank Jeff Dyck, Eamonn Conrad, Michael Moser and the team at CYTEC for all their support and abundance of phosphonium ionic liquid supplies.

Notes and references

AUTHOR INFORMATION

Corresponding Author

† Correspondence should be addressed to R.v.D., rik.vandeun@ugent.be, Tel. +32 (0)9264 4420 or P.N., p.nockemann@qub.ac.uk, Tel. +44 (0)28 9097 4475.

Author Contributions

The manuscript was written through contributions of all authors. All authors have given approval to the final version of the manuscript.

References

1 Wilkes, J.S.; Wasserscheid, P.; Welton, T. *Introduction*, Wiley-VCH Verlag GmbH & Co. KGaA, Weinheim, Germany, 2007.

2 Plechkova, N. V.; Seddon, K. R. Applications of ionic liquids in the chemical industry. *Chem. Soc. Rev.*, **2007**, *37*, 123–150.

3 Wellens, S.; Goovaerts, R.; Moeller, C.; Luyten, J.; Thijs, B.; Binnemans, K. Separation of cobalt and nickel using a thermomorphic ionic-liquid-based aqueous biphasic system. *Green Chem.*, 2013, **15**, 3160–3164.

4 Abai, M.; Atkins, M. P.; Hassan, A.; Holbrey, J. D.; Kuah, Y.; Nockemann, P.; Oliferenko, A. A.; Plechkova, N. V.; Rafeen, S.; Rahman, A. A. *et al.* An ionic liquid process for mercury removal from natural gas. *Dalton Trans.*, **2015**, *44*, 8617–8624.

5 Taubert, A.; Li, Z. Inorganic materials from ionic liquids. *Dalton Trans.*, **2007**, 723–727.

6 Freudenmann, D.; Wolf, S.; Wolff, M.; Feldmann, C. Ionic liquids: new perspectives for inorganic synthesis? *Angew. Chem. Int. Ed.*, **2011**, *50*, 11050–11060.

7 Yoshida, Y.; Saito, G. Design of functional ionic liquids using magneto- and luminescent-active anions. *Phys. Chem. Chem. Phys.*, **2010**, *12*, 1675–1684.

8 Estager, J.; Holbrey, J. D.; Swadzba-Kwasny, M. Halometallate ionic liquids – revisited. *Chem. Soc. Rev.*, **2014**, *43*, 847–886.

9 Estager, J.; Nockemann, P.; Seddon, K. R.; Swadzba-Kwasny, M.; Tyrrell, S. Validation of Speciation Techniques: A Study of Chlorozincate(II) Ionic Liquids. *Inorg. Chem.*, **2011**, *50*, 5258–5271.

10 Currie, M.; Estager, J.; Licence, P.; Men, S.; Nockemann, P.; Seddon, K. R.; Swadzba-Kwasny, M.; Terrade, C. Chlorostannate(II) Ionic Liquids: Speciation, Lewis Acidity, and Oxidative Stability. *Inorg. Chem.*, **2013**, *52*, 1710–1721.

11 Earle, M. J.; Seddon, K. R.; Adams, C. J.; Roberts, G. Friedel-Crafts reactions in room temperature ionic liquids. *Chem. Commun.*, **1997**, 2097–2098.

12 Peppel, T.; Köckerling, M.; Geppert-Rybczynska, M.; Ralys, R. V.; Lehmann, J. K.; Verevkin, S. P.; Heintz, A. Studies of physicochemical and thermodynamic properties of the paramagnetic 1-alkyl-3-methylimidazolium ionic liquids $(EMIm)_2[Co(NCS)_4]$ and $(BMIm)_2[Co(NCS)_4]$. *Angew. Chem. Int. Ed.*, **2010**, *49*, 7116–7119.

13 Osborne, S. J.; Wellens, S.; Ward, C.; Felton, S.; Bowman, R. M.; Binnemans, K.; Swadzba-Kwasny, M.; Gunaratne, H. Q. N.; Nockemann, P. Thermochromism and switchable paramagnetism of cobalt(II) in thiocyanate ionic liquids. *Dalton Trans.*, **2015**, *44*, 11286–11289.

14 Tyrrell, S.; Behrendt, G.; Liu, Y. W.; Nockemann, P. Zinc selenide nano- and microspheres via microwave-assisted ionothermal synthesis. *RSC Adv*, **2014**, *4*, 36110–36116.

15 Wang, L. J.; Lin, C. H. Synthesis and Application of Metal Ion Containing Ionic Liquids: A Brief Review. *Mini-Rev. Org. Chem.*, **2012**, *9*, 223–226.

16 Abbott, A. P.; Frisch, G.; Hartley, J.; Ryder, K. S. Processing of metals and metal oxides using ionic liquids. *Green Chem*, **2011**, *13*, 471–481.

17 Bäcker, T.; Breunig, O.; Valldor, M.; Merz, K.; Vasylyeva, V.; Mudring, A. V. In-Situ Crystal Growth and Properties of the Magnetic Ionic Liquid [C_2mim][$FeCl_4$]. *Cryst. Growth Des.*, **2011**, *11*, 2564–2571.

18 Nockemann, P.; Thijs, B.; Postelmans, N.; Van Hecke, K.; Van Meervelt, L.; Binnemans, K. Anionic Rare-Earth Thiocyanate Complexes as Building Blocks for Low-Melting Metal-Containing Ionic Liquids. *J. Am. Chem. Soc.*, **2006**, *128*, 13658–13659.

19 Borges, A. S.; Da Silva, J. G.; Ayala, J. D.; Dutra, J. D. L.; Speziali, N. L.; Brito, H. F.; Araujo, M. H. Synthesis, crystal structure and luminescence properties of the Ln(III)-picrate complexes with 1-ethyl-3-methylimidazolium as countercations. *Spectrochim. Acta, Part A*, **2014**, *117*, 718–727.

20 Mallick, B.; Balke, B.; Felser, C.; Mudring, A. V. Dysprosium room-temperature ionic liquids with strong luminescence and response to magnetic fields. *Angew. Chem. Int. Ed.*, **2008**, *47*, 7635–7638.

21 Tang, S.; Babai, A.; Mudring, A. V. Europium-Based Ionic Liquids as Luminescent Soft Materials. *Angew. Chem. Int. Ed.*, **2008**, *47*, 7631–7634.

22 Nockemann, P.; Beurer, E.; Driesen, K.; Van Deun, R.; Van Hecke, K.; Van Meervelt, L.; Binnemans, K. Photostability of a highly luminescent europium beta-diketonate complex in imidazolium ionic liquids. *Chem. Commun.*, 2005, 4354–4356.

23 Arenz, S.; Babai, A.; Binnemans, K.; Driesen, K.; Giernoth, R.; Mudring, A. V.; Nockemann, P. Intense near-infrared luminescence of anhydrous lanthanide(III) iodides in an imidazolium ionic liquid. *Chem. Phys. Let.*, **2005**, *402*, 75–79.

24 Lunstroot, K.; Nockemann, P.; Van Hecke, K.; Van Meervelt, L.; Gorller-Walrand, C.; Binnemans, K.; Driesen, K. Visible and Near-Infrared Emission by Samarium(III)-Containing Ionic Liquid Mixtures. *Inorg. Chem.*, **2009**, *48*, 3018–3026.

25 Prodius, D.; Macaev, F.; Lan, Y. H.; Novitchi, G.; Pogrebnoi, S.; Stingaci, E.; Mereacre, V.; Anson, C. E.; Powell, A. K. Evidence of slow relaxation of magnetization in dysprosium-based ionic liquids. *Chem. Commun.*, **2013**, *49*, 9215–9217.

26 Ji, S. P.; Tang, M.; He, L.; Tao, G. H. Water-Free Rare-Earth-Metal Ionic Liquids/Ionic Liquid Crystals Based on Hexanitratolanthanate(III) Anion. *Chem. - Eur. J.*, **2013**, *19*, 4452–4461.

27 Santos, E.; Albo, J.; Daniel, C. I.; Portugal, C. A. M.; Crespo, J. G.; Irabien, A. Permeability modulation of Supported Magnetic Ionic Liquid Membranes (SMILMs) by an external magnetic field. *J. Membr. Sci.*, **2013**, *430*, 56–61.

28 Decadt, R.; Van Hecke, K.; Depla, D.; Leus, K.; Weinberger, D.; Van Driessche, I.; Van Der Voort, P.; Van Deun, R. Synthesis, crystal structures, and luminescence properties of carboxylate based rare-earth coordination polymers. *Inorg. Chem.*, **2012**, *51*, 11623–11634.

29 Greenwood, N.; Earnshaw, A. *Chemistry of the Elements, Oxford: Butterworth-Heinemann*, 1997, p. 1243.

30 Stafford, G. R.; Hussey, C. L. *Advances in Electrochemical Science and Engineering*, Wiley-VCH Verlag GmbH, 2001.

31 Bhatt, A. I.; May, I.; Volkovich, V. A.; Collison, D.; Helliwell, M.; Polovov, I. B.; Lewin, R. G. Structural characterization of a lanthanum bistriflimide complex, $La(N(SO_2CF_3)_2)_3(H_2O)_3$, and an investigation of La, Sm, and Eu electrochemistry in a room-temperature ionic liquid, $[Me_3N_{(n)}Bu][N(SO_2CF_3)_2]$. *Inorg. Chem.* **2005,** *44* (14), 4934-4940.

32 Jagadeeswara Rao, C.; Venkatesan, K. A.; Nagarajan, K.; Srinivasan, T. G.; Vasudeva Rao, P. R. Electrochemical and thermodynamic properties of europium(III), samarium(III) and cerium(III) in 1-butyl-3-methylimidazolium chloride ionic liquid. *J. Nucl. Mat.* **2010,** *399* (1), 81-86.

33 Chou, L.-H.; Hussey, C. L. An Electrochemical and Spectroscopic Study of Nd(III) and Pr(III) Coordination in the 1-Butyl-1-methylpyrrolidinium Bis(trifluoromethylsulfonyl)imide Ionic Liquid Containing Chloride Ion. *Inorg. Chem.* **2014,** *53* (11), 5750-5758.

34 Zhang, Q. B.; Yang, C.; Hua, Y. X.; Li, Y.; Dong, P. Electrochemical preparation of nanostructured lanthanum using lanthanum chloride as a precursor in 1-butyl-3-methylimidazolium dicyanamide ionic liquid. *Phys. chem. chem. phys.*, **2015**, *17*, 4701–4707.

35 Yang, F. L.; Chen, C. A.; Wang, X. Y.; Zhang, G. K. Electrodeposition of Lanthanum in the Room Temperature Ionic Liquid MPPiNTf(2). *Rare Met. Mater. Eng.*, **2015**, *44*, 763–767.

36 Beale, A.M.; van der Eerden, A. M. J.; Jacques, S. D. M.; Leynaud, O.; O'Brien, M.G.; Meneau, F.: Nikitenko, S.; Bras, W.; Weckhuysen, B.M. A Combined SAXS/WAXS/XAFS Setup Capable of Observing Concurrent Changes Across the Nano-to-Micrometer Size Range in Inorganic Solid Crystallization Processes. *J. Am. Chem. Soc.*, **2006**, *128*, 12386–12387.

37 Nikitenko, S.; Beale, A. M.; van der Eerden, A. M. J.; Jacques, S. D. M.; Leynaud, O.; O'Brien, M. G.; Detollenaere, D.; Kaptein, R.; Weckhuysen, B. M.; Bras, W. Implementation of a combined SAXS/WAXS/QEXAFS set-up for time-resolved in situ experiments. IUCr, *J. Synchrotron Radiat.*, **2008**, *15*, 632–640.

38 Ressler, T. *WinXAS software for EXAFS data reduction*, 1997.

39 George, G. N.; Pickering, I. J. *EXAFSPAK: A suite of computer programs for analysis of X-ray absorption spectra*, SSRL, 1995.

40 Ravel, B.; Newville, M. ATHENA, ARTEMIS, HEPHAESTUS: data analysis for X-ray absorption spectroscopy using IFEFFIT. *J. Synchrotron Radiat.*, **2005**, *12*, 537–541.

41 Newville, M. EXAFS analysis using FEFF and FEFFIT. *J. Synchrotron Radiat.*, **2001**, *8*, 96–100.

42 Bain, G. A.; Berry, J. F. *J.* Diamagnetic Corrections and Pascal's Constants. *Chem. Educ.*, **2008**, *85*, 532.

43 Dolomanov, O. V.; Bourhis, L. J.; Gildea, R. J.; Howard, J. A. K.; Puschmann, H. Olex2: A complete structure solution, refinement and analysis program (2009). *J. Appl. Crystallogr*, **2009**, *42*, 339–341.

44 Sheldrick, G. M. Crystal structure refinement with SHELXL. *Acta Crystallogr. Sect. C Cryst. Struct. Commun.*, **2014**, *71*, 3–8.

Easily Accessible Rare-Earth-Containing Phosphonium Room-Temperature Ionic Liquids: EXAFS, Luminescence and Magnetic Properties

Jorge Alvarez-Vicente,[a] Sahra Dandil,[a,e] Dipanjan Banerjee,[c] H.Q. Nimal Gunaratne,[a] Suzanne Gray,[d] Solveig Felton,[d] Geetha Srinivasan,[a] Anna M. Kaczmarek,[b] Rik Van Deun,[*b] and Peter Nockemann[*a]

Graphical Abstract
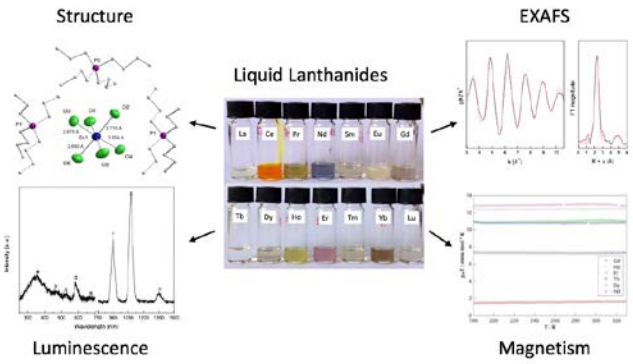
A range of liquid rare-earth chlorometallate complexes with alkyl-phosphonium cations has been synthesised and their structure (EXAFS), luminescence and magnetism has been determined.